Inorganic Chemistry
Article

Inorg. Chem. **2010**, *49*, 5591–5597 **5591**
DOI: 10.1021/ic100493t

Efficient Spin Filtering through Cobalt-Based Extended Metal Atom Chains

Vihar P. Georgiev and John E. McGrady*

Department of Chemistry, Inorganic Chemistry Laboratory, University of Oxford, South Parks Road, Oxford, OX1 3QR, United Kingdom

Received March 15, 2010

Density functional theory in conjunction with nonequilibrium Green's functions has been used to explore charge transport through the cobalt-based extended metal atom chain, $Co_3(dpa)_4(NCS)_2$. The isolated molecule has a doublet ground state, and the singly occupied σ nonbonding orbital proves to be the dominant transport channel, providing spin filtering efficiencies in excess of 90%. The metal chain differs from typical organic conductors in that the π orbitals that form the contact with the gold electrode are orthogonal to the transport channel. As a result, the rehybridization of these π levels by the applied electric field has only a minor impact on the current, allowing spin filtering to persist even at biases in excess of 1 V.

Introduction

Ever since Aviram and Ratner's seminal proposal of a molecular rectifier in 1974,[1] experimental and theoretical groups have sought to understand how current flows through single molecules, the ultimate goal being to construct devices based on molecular species.[2] In the intervening years, much progress has been made with unsaturated carbon-based materials, where the conjugated π system offers a high density of states near the Fermi level.[3] In the rather newer field of molecular spintronics, spin dependent current flow can, in principle, be achieved either by placing a diamagnetic molecular bridge between two ferromagnetic electrodes or, alternatively, by coupling a paramagnetic molecule to two diamagnetic electrodes.[4] In this second approach, the exchange splitting of the spin-up and spin-down manifolds in the molecular region causes them to align asymmetrically relative to the Fermi levels of the electrodes, allowing spin-polarized transport. Introducing radicals into organic architectures is, however, far from trivial, and so adapting them for applications in spintronics remains a considerable challenge.[5] Open-shell character is, in contrast, the norm in transition metal chemistry, and the incorporation of metal centers into a conduction channel offers obvious potential for distinguishing spin-up and spin-down currents. At the simplest level, this could involve a paramagnetic impurity in an otherwise diamagnetic metallic wire, and indeed da Silva and co-workers have recently highlighted the fact that even a single cobalt center in a one-atom-thick gold wire can act as an effective spin filter.[6] Min et al. have also computed substantial spin filtering efficiencies for alternating Au−Cr or Au−V wires absorbed on the outer wall of a B/N nanotube.[7] However, well-defined coordination complexes (as distinct from isolated metal atoms) clearly offer much greater potential for control and tuning of the density of states around the Fermi level, and a number of authors have explored the potential of both mono- and polymetallic systems in this context. For example, Baranger and co-workers[8] have recently illustrated how a cobaltocene unit (linked to gold electrodes through a −C≡C−S substituent on the cyclopentadienyl ring) can act as an efficient spin filter because only the vacant spin-β component of the SOMO lies close to the Fermi level. Moreover,

*To whom correspondence should be addressed. E-mail: john.mcgrady@chem.ox.ac.uk.

(1) Aviram, A.; Ratner, M. *Chem. Phys. Lett*. **1974**, *29*, 277.
(2) (a) Moore, G. E. *Electronics* **1965**, *38*, 114. (b) Reed, M. A.; Tour, J. *Sci. Am*. **2000**, *282*, 86. (c) Nitzan, A.; Ratner, M. A. *Science* **2003**, *300*, 1384.
(3) (a) Kim, W. Y.; Kim, K. S. *Acc. Chem. Res*. **2010**, *43*, 111. (b) Xue, Y.; Ratner, M. A. *Phys. Rev. B* **2004**, *69*, 085403. (c) Xue, Y.; Ratner, M. A. *Phys. Rev. B* **2003**, *68*, 115406. (d) Gonzalez, C.; Simón-Manso, Y.; Batteas, J.; Marquez, M.; Ratner, M. A.; Mujica, V. *J. Phys. Chem. B* **2004**, *108*, 18414. (e) Mujica, V.; Roitberg, A. E.; Ratner, M. A. *J. Chem. Phys*. **2000**, *112*, 6834. (f) Liang, G. C.; Ghosh, A. W.; Paulsson, M.; Datta, S. *Phys. Rev. B* **2004**, *69*, 115302.
(4) (a) Chappert, C.; Fert, A.; Van Dau, F. N. *Nat. Mater*. **2007**, *6*, 813. (b) Sanvito, S. *Nat. Mater*. **2007**, *6*, 803. (c) Sulczewski, G.; Sanvito, S.; Corey, M. *Nat. Mater*. **2009**, 693. (d) Camarero, J.; Coronado, E. *J. Mat. Chem*. **2009**, *19*, 1678. (e) Bibes, M.; Barthelemy, A. *Nat. Mater*. **2008**, *7*, 425.
(5) (a) Sugawara, T.; Minamoto, M.; Matsushita, M. M.; Nickels, P.; Komiyama, S. *Phys. Rev. B*. **2008**, *77*, 235316. (b) Chernick, E. T.; Mi, Q.; Vega, A. M.; Lockard, J. V.; Ratner, M. A.; Wasielewski, M. R. *J. Phys. Chem. B*. **2007**, *111*, 6728. (c) Sahin, H.; Senger, R. T. *Phys. Rev. B* **2008**, *78*, 205423. (d) Tagami, K.; Tsukuda, M. *J. Phys. Chem. B* **2004**, *108*, 6441. (e) Park, J.; Yang, H.; Park, K. -S.; Lee, E. -K. *J. Chem. Phys*. **2009**, *130*, 214103. (f) Girard, Y.; Yamamoto, T.; Watanabe, K. *e-J. Surf. Sci. Tech*. **2008**, *6*, 157. (g) Herrmann, C.; Solomon, G. C.; Ratner, M. A. *J. Am. Chem. Soc*. **2010**, *132*, 3682.
(6) Pontes, R. B.; da Silva, E. Z.; Fazzio, A.; da Silva, A. J. R. *J. Am. Chem. Soc*. **2008**, *130*, 9897.
(7) Min, Y.; Yao, K. L.; Liu, Z. L.; Gao, G. Y.; Cheng, H. G.; Zhu, S. C. *Nanotechnology* **2009**, *20*, 095201.
(8) Liu, R.; Ke, S. -H.; Yang, W.; Baranger, H. U. *J. Chem. Phys*. **2007**, *127*, 141104.

Published on Web 05/24/2010

coupling two such centers together via a diamagnetic bridge generates singlet and triplet diradical states that provide the basis, at least in principle, for a molecular switch.[9] The so-called sandwich molecular wires (SMWs), $[ML]_n$, where L is an aromatic ligand such as cyclopentadienyl,[10,11] benzene,[12] borazine,[13] or cyclooctatetraenyl[14] have also been studied extensively in the context of electron transport properties. In these systems, the M···M axis lies along the transport direction, and the contact to the electrode is established either directly through the metal atom itself or through the π system of the aromatic ring. A logical extension is to employ extended three-dimensional arrays of paramagnetic centers such as are present in single molecule magnets (SMMs),[15−17] and Sanvito et al. have recently highlighted how bias-induced rehybridization of orbitals can have a substantial impact on the transmission channels in a Mn_{12} cluster.[18]

The metallocene and SMM complexes described in the previous paragraph are members of a diverse and technologically important class of metal clusters whose defining feature is that the communication between the metal centers occurs through superexchange interactions rather than by direct covalent overlap of the metal orbitals. The chemistry of covalent metal−metal bonds is now a relatively mature subject, and the discovery of the quadruple bond in $[Re_2Cl_8]^{2-}$ in the late 1960s was a landmark that has contributed greatly to our understanding of bonding.[19] Rather more recently, the portfolio of known bond multiplicities has been extended to five with the discovery of ultrashort quintuple Cr−Cr bonds.[20,21] These systems have naturally excited considerable attention in the theoretical community, not least because the very different electronic structures of the linear and *trans*-bent isomers of Ar−Cr−Cr−Ar provide a switching mechanism that could support on/off current ratios ($I_{\text{trans-bent}}/I_{\text{linear}}$)

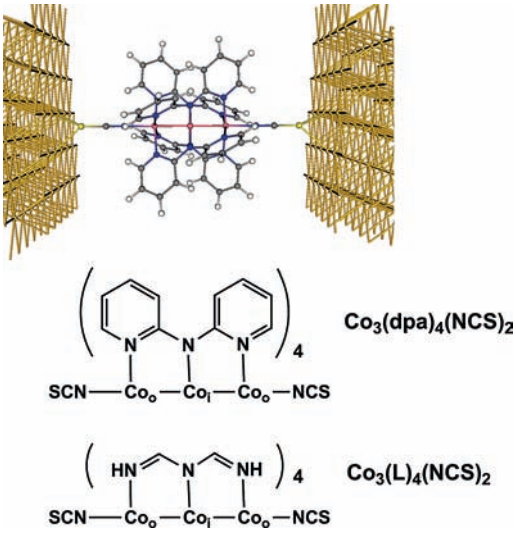

Figure 1. Structure of the $Co_3(dpa)_4(NCS)_2$ EMAC (dpa = dipyridylamide) and the model ligand, L, used in this study. The subscripts i and o refer to inner and outer cobalt centers, respectively.

of the order of 100.[22] While the quintuple bond remains somewhat exotic, metal−metal bonds of orders one through four are well-known stable entities, and the presence near the Fermi level of molecular orbitals of σ, π, and δ symmetry (with respect to the M−M axis) offers, at least in principle, a diverse range of transport channels. Among the many classes of metal−metal bonded systems, the family of *E*xtended *M*etal *A*tom *C*hains (EMACs), based on chains of metal atoms supported by helical arrays of polypyridylamido ligands (Figure 1), provides a visually appealling (although perhaps somewhat superficial) resemblance to a macroscopic wire.[23] The chemistry of these systems has been developed extensively in the groups of Peng[24] and Cotton,[25] and chains containing up to nine metal atoms[26] are now well characterized. More importantly, in the context of electron transport, examples are known for metals with widely differing d-electron counts and metal−metal bond types. Thus, for example, the d^7 configuration of Co(II) means that σ bonding prevails in cobalt chains, while their d^4 Cr(II) counterparts feature strong multiple bonds involving σ, π, and δ components which can be either localized in alternating Cr−Cr pairs or delocalized along the entire chain.[23] The structural and magnetochemical properties[27] of the $Co_3(dpa)_4Cl_2$ chains (dpa = dipyridylamide) are particularly intriguing, as these systems provide one of the few well-defined examples of polymorphism, where a molecule can exist in two distinct forms which differ only in the lengths of one or more bonds. We have recently shown that this remarkable structural chemistry can be understood in terms of a rather complex

(9) (a) Liu, R.; Ke, S. -H.; Baranger, H. U.; Yang, W. *Nano Lett*. **2005**, *5*, 1959. (b) Baadji, N.; Piacenze, M.; Tugsuz, T.; Sala, F. D.; Maruccio, G.; Sanvito, S. *Nat. Mater*. **2009**, *8*, 813.
(10) Wang, L.; Cai, Z.; Wang, J.; Lu, J.; Luo, G.; Lai, L.; Zhou, J.; Qin, R.; Gao, Z.; Yu, D.; Li, G.; Mei, W. N.; Sanvito, S. *Nano Lett*. **2008**, *8*, 3640.
(11) (a) Wu, J.-C.; Wang, X.-F.; Zhou, L.; Da, H.-X.; Lim, K. H.; Yang, S.-W.; Li, Z.-Y. *J. Phys. Chem. C* **2009**, *113*, 7913. (b) Zhou, L.; Yang, S.-Y.; Ng, M.-F.; Sullivan, M. B.; Tan, V. B. C.; Shen, L. *J. Am. Chem. Soc*. **2008**, *130*, 4023.
(12) (a) Maslyuk, V. V.; Bagrets, A.; Meded, V.; Arnold, A.; Evers, F.; Brandbyge, M.; Bredow, T.; Mertig, I. *Phys. Rev. Lett*. **2006**, *97*, 097201. (b) Koleini, M.; Paulsson, M.; Brandbyge, M. *Phys. Rev. Lett*. **2007**, *98*, 197202. (c) Xiang, H.; Yang, J.; Hou, J. G.; Zhu, Q. *J. Am. Chem. Soc*. **2006**, *128*, 2310.
(13) (a) Mallajosyula, S. S.; Parida, P.; Pati, S. K. *J. Mat. Chem*. **2009**, *19*, 1761. (b) Zhu, L.; Wang, J. *J.Phys. Chem. C*. **2009**, *113*(20), 8767.
(14) Xu, K.; Huang, J.; Lei, S.; Su, H.; Boey, F. Y. C.; Li, Q.; Yang, J. *J. Chem. Phys*. **2009**, *131*, 104704.
(15) (a) Heersche, H. B.; de Grrot, Z.; Folk, J. A.; van der Zant, H. S.; Romeike, C.; Wegewijs, M. R.; Zobbi, L.; Barreca, D.; Tondello, E.; Cornia, A. *Phys. Rev. Lett*. **2006**, *96*, 206801. (b) Jo, M.-H.; Grose, J. E.; Baheti, K.; Deshmukh, M. M.; Sokol, J. J.; Rumberger, E. M.; Hendrickson, D. N.; Long, J. R.; Park, H.; Ralph, D. C. *Nano Lett*. **2006**, *6*, 2014.
(16) Barraza-Lopez, S.; Park, K.; Garcia-Suarez, V.; Ferrer, J. *J. Appl. Phys*. **2009**, *105*, 07E309.
(17) Boani, L.; Wernsdorfer, W. *Nat. Mater*. **2008**, *7*, 179.
(18) Pemmeraju, D. D.; Rungeer, I.; Sanvito, S. *Phys. Rev. B* **2009**, *80*, 104422.
(19) Cotton, F. A.; Curtis, N. F.; Harris, C. B.; Johnson, B. F. G.; Lippard, S. J.; Mague, J. T.; Robinson, W. R.; Wood, J. S. *Science* **1964**, *145*, 1305.
(20) Nguyen, T.; Sutton, A. D.; Brynda, M.; Fettinger, J. C.; Long, G. J.; Power, P. P. *Science* **2005**, *310*, 844.
(21) (a) Kreisel, K. A.; Yap, G. P. A.; Dmitrenko, O.; Landis, C. R.; Theopold, K. H. *J. Am. Chem. Soc*. **2007**, *129*, 14162. (b) Noor, A.; Wagner, F. R.; Kempe, R. *Angew. Chem., Int. Ed*. **2008**, *47*, 7246.
(22) Huang, J.; Li, Q.; Ren, H.; Su, H.; Yang, J. *J. Chem. Phys*. **2006**, *125*, 184713.
(23) Berry, J. F.; Cotton, F. A.; Murillo, C. A.; Walton, R. A. *Multiple Bonds Between Metal Atoms*; Springer: New York, 2005.
(24) (a) Liu, I. P.-C.; Wang, W.-Z.; Peng, S.-M. *Chem. Commun*. **2009**, 4323. (b) Cheng, C.-H.; Hung, R.-D.; Wang, W.-Z.; Peng, S.-M.; Chia, C.-I. *ChemPhysChem*. **2010**, *11*(2), 466.
(25) Cotton, F. A. *Inorg. Chem*. **1998**, *37*, 5710.
(26) Ismailov, R.; Weng, W.-Z.; Wang, R.-R.; Huang, Y.-L.; Yeh, C.-Y.; Lee, G.-H.; Peng, S.-M. *Eur. J. Inorg. Chem*. **2008**, 4290.
(27) (a) Yang, E.-C.; Cheng, M.-C.; Tsai, M.-S.; Peng, S.-M. *J. Chem. Soc., Chem. Commun*. **1994**, 2377. (b) Clérac, R.; Cotton, F. A.; Daniels, L. M.; Dunbar, K. R.; Kirschbaum, K.; Murillo, C. A.; Pinkerton, A. A.; Schultz, A. J.; Wang, X. *J. Am. Chem. Soc*. **2000**, *122*, 6226. (c) Clérac, R.; Cotton, F. A.; Daniels, L. M.; Dunbar, K. R.; Murillo, C. A.; Wang, X. *Inorg. Chem*. **2001**, *40*, 1256.

temperature-dependent redistribution of charge density between the σ, π, and δ components of the Co−Co−Co manifold,[28] an observation that leads naturally to the question of how such a system might behave under applied bias in a putative molecular electronic device.

Peng and co-workers have addressed this question by using both STM and c-AFM techniques to measure the conductance of thiocyanate-capped oligo-α-pyridylamido chains containing three and five metal atoms.[29] The conductance increases in the order Ni < Co < Cr, suggesting that the metal core plays a defining role in electron transport. Perhaps most remarkably, the pentachromium system apparently undergoes stochastic switching between distinct conducting and nonconducting states, perhaps corresponding to the localized and delocalized distributions, respectively, of Cr−Cr multiple bonds alluded to earlier. In a separate series of experiments on the chloride-capped Ni_3 and Cu_3 analogues, where the coupling to the gold electrodes is rather weaker, Yao and co-workers have shown clear evidence for Coulomb blockade behavior.[30] The further development of these systems in the context of molecular spintronics will necessarily rely on a detailed understanding of how the interrelated issues of electronic configuration, metal−metal bonding, and spin state combine to control the flow of current. Jin and co-workers have computed the conductance of the trimetallic cobalt, chromium, and nickel chains using an extended Hückel framework and concluded that the antibonding combination of d_{z^2} orbitals on the metal centers dominates charge transport.[31] However, the extended Hückel model precludes any consideration of spin polarization effects that are integral to spin filtering. In this contribution, we use density functional theory,[32] where the lineup of the Fermi level of the gold electrodes relative to the orbitals of the channel is determined self-consistently, to explore the behavior of the symmetric form of the prototypical EMAC, $Co_3(dpa)_4(NCS)_2$, under applied bias. We show that the spin density distribution characteristic of the doublet ground state of the isolated molecule is retained even after absorption onto the gold electrodes, and the resultant exchange splitting of majority- and minority-spin manifolds supports spin filtering efficiencies of up to 90% at low bias. Most remarkably, a spin polarized current is maintained even at biases that significantly exceed the magnitude of the exchange splitting because the levels in the channel become pinned to the potential of the drain; as a result, the majority-spin channels remain largely outside the bias window.

Computational Methods

The spin-dependent electron transport properties of the cobalt-based EMAC were computed using the Atomistic-Toolkit software package, ATK2008.[33,34] The methodology combines a density functional theory treatment of the electronic structure with the Keldysh nonequilibrium Green's function approach to simulating coherent transport under nonequilibrium conditions.[35] The scattering region, $[Au_{32}]$-$Co_3(L)_4(NCS)_2$-$[Au_{48}]$, contains the EMAC sandwiched between two and three 4×4 layers of the Au(111) surface of the source and drain electrodes, respectively, with the sulfur atoms of the two NCS ligands located in hollow sites with Au−S distances of 2.52 Å. The Perdew Burke Ernzerhof (PBE) functional[36] was used throughout in conjunction with numerical basis sets of double-ζ + polarization (DZP) quality on all atoms other than the nitrogens, where an additional polarization functional was added (DZDP). Core electrons were described by norm-conserving pseudopotentials.[37] The geometry of $Co_3(dpa)_4(NCS)_2$ in the scattering region was optimized in its doublet ground state using ADF2008[38] with the same PBE functional and a triple-ζ quality basis of Slater-type functions on cobalt and double-ζ + polarization elsewhere (a full set of Cartesian coordinates for the two-probe system is provided in the Supporting Information). In order to reduce the dimensions of the unit cell in the directions perpendicular to the transport direction, the dipyridylamido ligand was simplified by removing the bulk of the pyridyl rings and capping the unsaturated valences at C and N with hydrogen atoms at 1.1 Å and 1.0 Å, respectively ($Co_3(L)_4$-$(NCS)_2$, Figure 1). Although truncating a ligand across an aromatic bond in this way is clearly not ideal, test calculations suggest that this simplification does not perturb the equilibrium electronic structure of the isolated molecule to any significant extent. The electronic structure of the two-probe systems at equilibrium was converged using a 350 Ry mesh cutoff, a finite temperature of 300 K at the electrodes, and the density matrix constraint at the electrodes. Sampling of the Brillouin zone was performed using a Monkhorst-Pack grid[39] with 300 k-points along the transport direction. The molecular orbitals in the scattering region are the eigenfunctions of

(28) (a) Pantazis, D. A.; McGrady, J. E. *J. Am. Chem. Soc.* **2006**, *128*, 4128. (b) Pantazis, D. A.; Murillo, C. A.; McGrady, J. E. *Dalton Trans.* **2008**, 608. (c) McGrady, J. E.; Pantazis, D. A. *Chemtracts Inorg. Chem.* **2005**, *18*, 629.

(29) (a) Lin, S. Y.; Chen, I. W. P.; Chen, C. H.; Hsieh, M.-H.; Yeh, C. Y.; Lin, T. W.; Chen, Y. H.; Peng, S.-M. *J. Phys. Chem. B* **2004**, *108*, 959. (b) Chen, P.; Fu, M.-D.; Tseng, W. H.; You, J.-Y.; Wu, S.-H.; Ku, C.-J.; Chen, C.-H.; Peng, S.-M. *Angew. Chem., Int. Ed.* **2006**, *45*, 5814. (c) Shin, K.-N.; Huang, M. J.; Lu, H. G.; Fu, M.-D.; Kuo, C.-K.; Huang, G.-C.; Lee, G.-H.; Chen, C.-H.; Peng, S.-M. *Chem. Commun.* **2010**, *46*, 1338.

(30) Chae, D.-H.; Berry, J. F.; Jung, S.; Cotton, F. A.; Murillo, C. A.; Yao, Z. *Nano Lett.* **2006**, *6*, 165.

(31) (a) Hsu, L. Y.; Huang, Q. R.; Jin, B.-Y. *J. Phys. Chem. C.* **2008**, *112*, 10538. (b) Tsai, T. W.; Huang, Q.-R.; Peng, S.-M.; Jin, B.-Y. *J. Phys. Chem. C* **2010**, *114*, 3641.

(32) (a) Kim, W. Y.; Choi, Y. C.; Min, S. K.; Cho, Y.; Kim, K. S. *Chem. Soc. Rev.* **2009**, *38*, 2319. (b) Koentopp, M.; Chang, C.; Burke, K.; Car, R. *J. Phys.: Condens. Matter* **2008**, *20*, 083203.

(33) QuantumWise. http://www.quantumwise.com/ (accessed May 2010).

(34) (a) Brandbyge, M.; Mozos, J.-L.; Ordejon, P.; Taylor, P.; Stokbro, K. *Phys. Rev. B* **2002**, *65*, 165401. (b) Soler, J. M.; Artacho, E.; Gale, J. D.; Garcia, A.; Unquera, J.; Ordejon, P.; Sanchez-Portal, D. *J. Phys.: Condens. Matter* **2002**, *14*, 2745. (c) Taylor, J.; Guo, H.; Wang, J. *Phys. Rev. B* **2001**, *63*, 245407.

(35) (a) Datta, S. *Electron Transport in Mesoscopic Systems*; Cambridge University Press: Cambridge, U. K., 1997. (b) Datta, S. *Quantum Transport: Atom to Transistor*; Cambridge University Press: Cambridge, U. K., 2005. (c) Jortner, J.; Nitzan, A.; Ratner, M. A. *Lecture Notes in Physics, Introducing Molecular Electronics*; Springer: New York, 2005; Vol. *14*. (d) Lindsay, S. *Farad. Disc.* **2006**, *131*, 403.

(36) Perdew, J. P.; Burke, K.; Ernzerhof, M. *Phys. Rev. Lett.* **1996**, *77*, 3865.

(37) Troullier, N.; Martins, J. L. *Phys. Rev. B* **1991**, *43*, **1993**.

(38) Baerends, E. J.; Autschbach, J.; Bérces, A.; Bickelhaupt, F. M.; Bo, C.; Boerrigter, P. M.; Cavallo, L.; Chong, D. P.; Deng, L.; Dickson, R. M.; Ellis, D. E.; van Faassen, M.; Fan, L.; Fischer, T. H.; Fonseca Guerra, C.; van Gisbergen, S. J. A.; Götz, A. W.; Groeneveld, J. A.; Gritsenko, O. V.; Grüning, M.; Harris, F. E.; van den Hoek, P.; Jacob, C. R.; Jacobsen, H.; Jensen, L.; van Kessel, G.; Kootstra, F.; Krykunov, M. V.; van Lenthe, E.; McCormack, D. A.; Michalak, A.; Neugebauer, J.; Nicu, V. P.; Osinga, V. P.; Patchkovskii, S.; Philipsen, P. H. T.; Post, D.; Pye, C. C.; Ravenek, W.; Rodriguez, J. I.; Ros, P.; Schipper, P. R. T.; Schreckenbach, G.; Snijders, J. G.; Solà, M.; Swart, M.; Swerhone, D.; te Velde, G.; Vernooijs, P.; Versluis, L.; Visscher, L.; Visser, O.; Wang, F.; Wesolowski, T. A.; van Wezenbeek, E. M.; Wiesenekker, G.; Wolff, S. K.; Woo, T. K.; Yakovlev, A. L.; Ziegler, T. *ADF2008.01*; SCM, Theoretical Chemistry, Vrije Universiteit: Amsterdam, The Netherlands. http://www.scm.com (accessed May 2010).

(39) Monkhorst, H. J.; Pack, J. D. *Phys. Rev. B* **1976**, *13*, 5188.

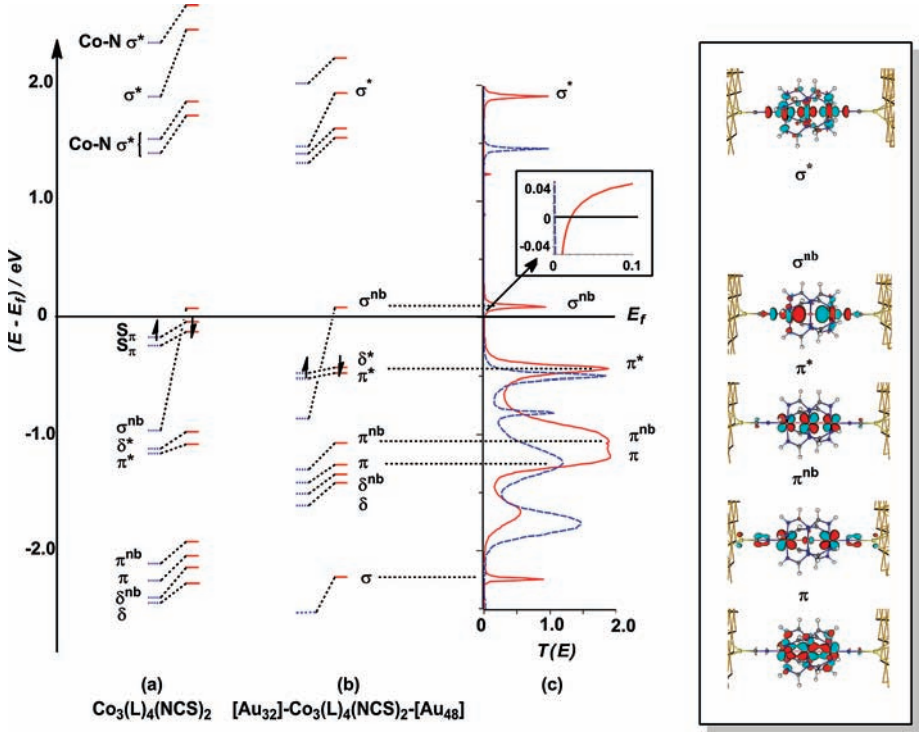

Figure 2. Molecular orbital diagram for (a) isolated $Co_3(L)_4(NCS)_2$, (b) $Co_3(L)_4(NCS)_2$ sandwiched between gold electrodes, and (c) the zero-bias transmission spectrum for $[Au_{32}]$-$Co_3(L)_4(NCS)_2$-$[Au_{48}]$ (inset is an expansion of the region around the Fermi level). Spin-α and spin-β components are shown in blue (dashed) and red, respectively.

the molecular projected self-consistent Hamiltonian (MPSH). The current is computed using the Landauer[40] formula:

$$I_\sigma(V) = \frac{e}{h}\int_{E=-\infty}^{\infty} T_\sigma(E,V)(f(\varepsilon,\mu_L) - f(\varepsilon,\mu_R))\,dE$$

where $T_\sigma(E,V)$ is the (spin- and voltage-dependent) transmission coefficient and $f(\varepsilon,\mu_L)$ and $f(\varepsilon,\mu_R)$ are the Fermi functions of the two electrodes with chemical potentials $\mu_L = -eV/2$ and $\mu_R = eV/2$, respectively. The subscript σ denotes the spin component (α or β). In the calculation of current, the bias window was sampled at intervals of 0.005 eV, corresponding to 100, 200, 300, and 400 integration points for 0.5, 1.0, 1.5, and 2.0 V, respectively. At zero bias, the conduction, $G_\sigma(0)$, is given by the expression:

$$G_\sigma(0) = \left(\frac{dI}{dV}\right)_{v=0} = \frac{e^2}{h}T_\sigma(E_f,0)$$

Results

Equilibrium Properties. We[28] and others[41,42] have discussed the electronic structure of both the symmetric and unsymmetric forms of the closely related tricobalt chains $Co_3(dpa)_4Cl_2$ in some detail previously, so our purpose here is simply to review the key features that relate directly to the electron transport properties to be described later. A schematic molecular orbital diagram for the doublet ground state of the symmetric form of the NCS-capped species, $Co_3(L)_4(NCS)_2$, is shown in Figure 2a, while a Mulliken population analysis is summarized in Table 1. In Figure 2a, all orbitals of the isolated molecule have been arbitrarily shifted such that the spin-β component of the σ^{nb} SOMO is coincident with the corresponding orbital in the two-probe system, $[Au_{32}]$-$Co_3(L)_4(NCS)_2$-$[Au_{48}]$ (*vide infra*). The molecular orbital array for the corresponding system with the complete dpa ligand (Figure S1, Supporting Information) is very similar, confirming that our simplified ligand does not perturb the underlying electronic structure of the metal chain to any great extent. The basic features of the molecular orbital array are similar to those for the chloride-capped analogue:[28] between −1.0 and −2.5 eV lies a band of nine Co-based levels made up of linear combinations of the t_{2g} orbitals of the individual octahedra, three with local π symmetry (π, π^{nb}, and π^*), each of which is doubly degenerate, and three with local δ symmetry, δ, δ^{nb}, and δ^*. The highest occupied orbital has π symmetry and is localized primarily on the sulfur centers (denoted S_π in Figure 2a). Bracketing the occupied π/δ band are σ bonding and nonbonding linear combinations of the Co d_{z^2} orbitals, the latter being singly occupied in the

Table 1. Mulliken populations $\rho(\alpha+\beta)$ and spin densities $\rho(\alpha-\beta)$ for $Co_3(L)_4(NCS)_2$ and $[Au_{32}]$-$Co_3(L)_4(NCS)_2$-$[Au_{48}]$

		S	C	N	Co_o	Co_i
$Co_3(L)_4(NCS)_2$	$\rho_{\alpha+\beta}$	6.24	4.34	4.93	8.74	8.66
	$\rho_{\alpha-\beta}$	0.08	0.00	0.06	0.43	−0.05
$[Au_{32}]$-$Co_3(L)_4(NCS)_2$-$[Au_{48}]$	$\rho_{\alpha+\beta}$	6.36	4.26	4.84	8.69	8.65
	$\rho_{\alpha-\beta}$	0.00	0.00	0.04	0.50	−0.10

(40) (a) Landauer, R. *IBM J. Res. Dev.* **1957**, *1*, 233. (b) Landauer, R. *Philos. Mag.* **1970**, *21*, 863.
(41) (a) Rohmer, M.-M.; Bénard, M. *J. Am. Chem. Soc.* **1998**, *120*, 9372. (b) Rohmer, M.-M.; Strich, A.; Bénard, M.; Malrieu, J.-P. *J. Am. Chem. Soc.* **2001**, *123*, 9126. (c) Rohmer, M.-M.; Bénard, M. *Chem. Soc. Rev.* **2001**, *30*, 340.
(42) Poulsen, R. D.; Overgaard, J.; Schulman, A.; Østergaard, C.; Murillo, C. A.; Spackman, M. A.; Iversen, B. B. *J. Am. Chem. Soc.* **2009**, *131*, 7580.

ground state, giving a net Co−Co bond order of 0.5 and substantial Mulliken spin densities on the outer cobalt centers (Co_o, $\rho_{\alpha-\beta} = 0.43$). At higher energy, we find three vacant Co−N σ antibonding orbitals that have δ symmetry with respect to the Co−Co axis, along with the antibonding σ^* orbital which lies over 2 eV above σ^{nb}. The exchange splitting stabilizes the entire spin-α manifold, but its magnitude is highly orbital-dependent and is most apparent in the σ manifold. Thus, the spin-α and spin-β components of the σ^{nb} and σ^* orbitals are separated by ~1 eV, while the π^* orbital, which has rather little amplitude on the terminal Co centers, is split by only ~0.05 eV.

Turning to the two-probe system (Figure 2b) where the molecule is sandwiched between two gold electrodes, the basic features of the electronic structure are very similar, suggesting that the molecule/electrode interaction does not perturb the former to any great extent. Thus, an excess of approximately one spin-α electron is maintained in the molecular region and remains localized on the outer cobalt centers. A small amount of negative charge accumulates at the sulfur atoms of the thiocyanate ligand at the expense of the nitrogen and carbon, indicating a shift from the −N=C=S resonance structure toward N≡C−S−, but otherwise the electron density distribution remains unchanged. The manifold of metal-based levels becomes compressed into a narrower energy window than in the isolated molecule, but the general pattern of bonding, nonbonding, and antibonding combinations of σ, π, and δ symmetry remains intact, the only major change being the removal from the frontier region of the degenerate S_π levels which mediate the Au−S bonds.

In terms of transport properties, the central issues are the extent to which the molecular levels discussed above form effective transmission channels and how these channels align relative to the Fermi levels of the gold electrodes. The transmission functions for the spin-α and spin-β manifolds at zero bias, shown in Figure 2c, map directly onto the orbital energies for the scattering region, with three intense peaks with $T(E) \sim 2.0$ corresponding to the doubly degenerate channels of π symmetry, π, π^{nb}, and π^*. All three of these are broadened by the contact with the gold electrode due to π character on the terminal sulfur atoms, dramatically so in the case of the π^{nb} level where the sulfur contribution is highest. The corresponding (nondegenerate) σ bonding, nonbonding, and antibonding levels (σ, σ^{nb}, and σ^*) have a maximum $T(E) \sim 1$ and are rather less broadened as a result of having lower amplitude on the sulfur terminii. The remainder of the metal-based orbitals have δ symmetry with respect to the Co−Co axis and so couple only weakly to the electrode surface. The most striking feature is that the occupied spin-α and vacant spin-β components of the σ^{nb} orbital are distributed asymmetrically relative to the Fermi level of the gold electrodes: the former lies 0.85 eV below E_f, while the latter lies only 0.20 eV above it. As a result, the zero-bias conduction is dominated almost entirely by the spin-β channel (see inset in Figure 2): $G_\alpha = 0.03\ \mu S$, $G_\beta = 0.57\ \mu S$, $G_{tot} = 0.60\ \mu S$, corresponding to a spin-filtering efficiency (SFE, defined at 0 V as $(G_\beta - G_\alpha)/(G_\beta + G_\beta) \times 100\%$) of 90%, comparable to values computed for ferrocene-based SMWs.[11] Analysis of the transmission channels reveals that, while almost all the spin-β current is carried through the σ^{nb} channel, the (much smaller) spin-α conductance is dominated by the broader π^* band. The computed total conductance of 0.60 μS is very similar to the value of 0.53 μS measured by Peng and co-workers using STM (at 0.025 V).[29] Conductance values are typically overestimated by an order of magnitude using DFT-based formalisms[32] a trend that has been ascribed variously to the limitations of DFT (in particular the failure to account for the self-interaction energy) or to the idealized contact geometry. Given the simplifications associated with our model, most notably the truncation of the ligand and the choice of a hollow site on the gold surface (which will necessarily maximize the coupling), this close agreement is therefore probably a result, at least in part, of error cancellation, and a comparison across a broader range of compounds is necessary before definitive conclusions regarding the accuracy of the model can be made. Nevertheless, it suggests that our computational model is capturing the essential features of the two-probe system at equilibrium. Our computed values are 2 orders of magnitude larger than those calculated by Jin and co-workers using extended Hückel theory.[31] The origin of this discrepancy probably lies in the rather different alignment of molecular orbitals with respect to the electrode Fermi levels in the two methods: in reference 31a, the σ^* channel was proposed to be the major carrier, whereas our calculations suggest that this orbital lies almost 2 eV above E_f, in which case it will make a negligible contribution to current flow. We note in this context that the minimal charge transfer associated with absorption of the molecule on the gold surfaces discussed above appears inconsistent with a close alignment of the electrode Fermi levels with the high-lying σ^*, as this would inevitably result in double occupation of the much lower-lying σ^{nb} orbital (i.e., complete one-electron reduction of the molecule).

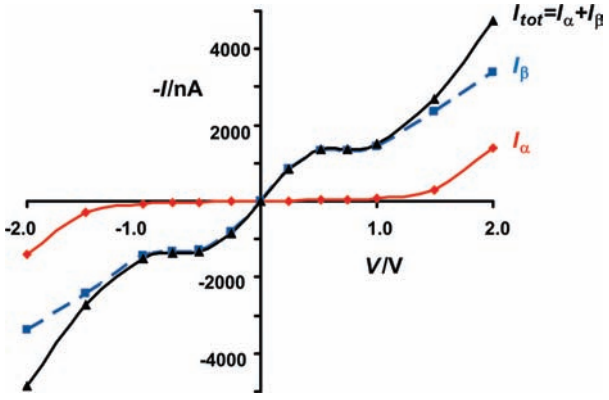

Figure 3. Computed current/voltage characteristics in $[Au_{32}]$-$Co_3(L)_4(NCS)_2$-$[Au_{48}]$.

Device Out of Equilibrium. The transmission spectrum discussed in the previous section confirms that the strong exchange splitting of the σ^{nb} orbital, which leaves only the spin-β component near the Fermi level, provides a basis for high SFEs, at least at low bias. The computed current/voltage characteristics shown in Figure 3 confirm that the current flow is dominated almost entirely by the minority-spin channel up to biases of ±1.0 V, with a SFE, defined at finite bias as $(I_\beta - I_\alpha)/(I_\beta + I_\alpha) \times 100\%$, well in excess of 90%. Beyond this plateau, both spin-α

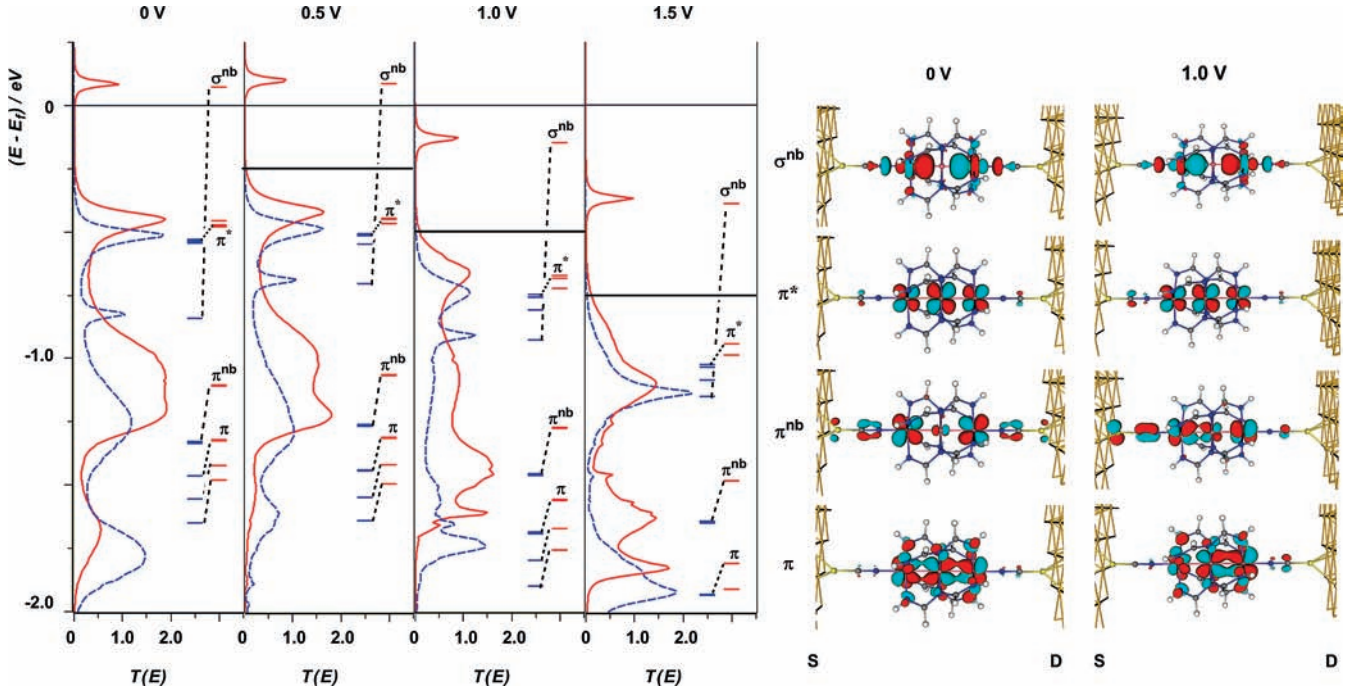

Figure 4. Changes in transmission spectrum as a function of applied bias (0−1.5 V) for $[Au_{32}]$-$Co_3(L)_4(NCS)_2$-$[Au_{48}]$. Red and blue (dashed) lines denote spin-β and spin-α components, respectively. Horizontal black lines for 0.5, 1.0, and 1.5 V mark the potential of the drain electrode. MPSH orbitals for the π, π^{nb}, π^*, and σ^* channels at 0 and 1.0 V are also shown for comparison.

and spin-β manifolds begin to contribute to the current, although the latter remains dominant even at 2.0 V. In the linear response limit (where $T(E)$ is assumed to be bias-independent), Figure 2c suggests that transmission through the broader π^* channel should start to dominate at biases in excess of ~0.75 V, and the small exchange splitting within this level means that the SFE should be effectively eliminated. To understand why this is apparently not the case, we need to consider how the transmission spectrum evolves as a function of bias. Transmission spectra, $T(E)$, for 0, 0.5, 1.0, and 1.5 V are collected in Figure 4, where the energies of the orbitals in the scattering region are also shown for comparison. Bias-induced changes in electron density, along with the profile of the electrostatic potential, are compared for 0.25 and 1.0 V in Figure 5.

At 0.25 V, only the vacant spin-β component of the σ^{nb} orbital falls within the bias window, and as a result there is a marginal buildup of spin-β electron density in the Co_3 region (see Figure 5a). Consistent with this, the potential profile drop is localized largely at the nitrogen atom of the −NCS ligand adjacent to the drain, and the peaks in the transmission spectrum shift marginally upward in energy. Beyond 0.5 V, however, the transmission spectra become highly bias-dependent, with all peaks shifting downward, following the potential of the drain. This pinning of the molecular levels to the drain occurs because the bias window begins to capture the upper tail of the occupied π^* channel, resulting in a depletion of charge (both spin-α and spin-β) which extends across the molecule to the cobalt adjacent to the source, where the conjugation is interrupted by the Co−NCS bond. As a result, the profile of the electrostatic potential shows a more pronounced drop across the source-molecule junction in this case.[43]

The fingerprint of the π^* level is apparent in Figure 5b in the regions of charge depletion in both spin-α and spin-β density at the cobalt adjacent to the drain. At the same point that the peaks in the transmission spectrum begin to follow the potential of the drain, their shapes also become highly bias-dependent: those corresponding to the three π channels (π, π^{nb}, and π^*) become substantially broader and weaker while the σ manifold remains essentially unperturbed. The large polarizability of the π manifold arises because the three components, π^*, π^{nb}, and π, span less than 1 eV, as a result of which they are substantially mixed by the applied electric field, an effect that has been noted in related systems.[18,44] Thus, while all three orbitals necessarily have equal amplitude on the two terminal cobalt centers at 0 V, at 1.0 V the π^* orbital becomes somewhat localized on the source side, while its bonding counterpart has greater amplitude adjacent to the drain (Figure 4). This rehybridization reduces the ability of the π channels to transport charge, and the corresponding peak heights in the transmission spectrum are dramatically reduced. In marked contrast, the σ^{nb} orbital is energetically isolated from both its bonding and antibonding counterparts, which lie approximately 2 eV lower and higher, respectively. The σ framework is therefore substantially less polarizable than its π counterpart, and the σ^{nb} channel remains unperturbed even up to 2.0 V. The net result of these bias-induced changes in the distribution of the orbitals in the molecular region is that the resonances due to the spin-α and spin-β components of the π^* channel are largely quenched above 1.0 V, allowing the spin-β component of the σ^{nb} channel to continue to dominate charge transport and hence to maintain high spin filtering efficiencies.

(43) Garcia-Suarez, V.; Lambert, C. J. *Nanotechnology* **2008**, *19*, 455203.

(44) Sengupta, S.; Lakshmi, S.; Pati, S. K. *J. Phys.: Condens. Matter* **2006**, *18*, 9189.

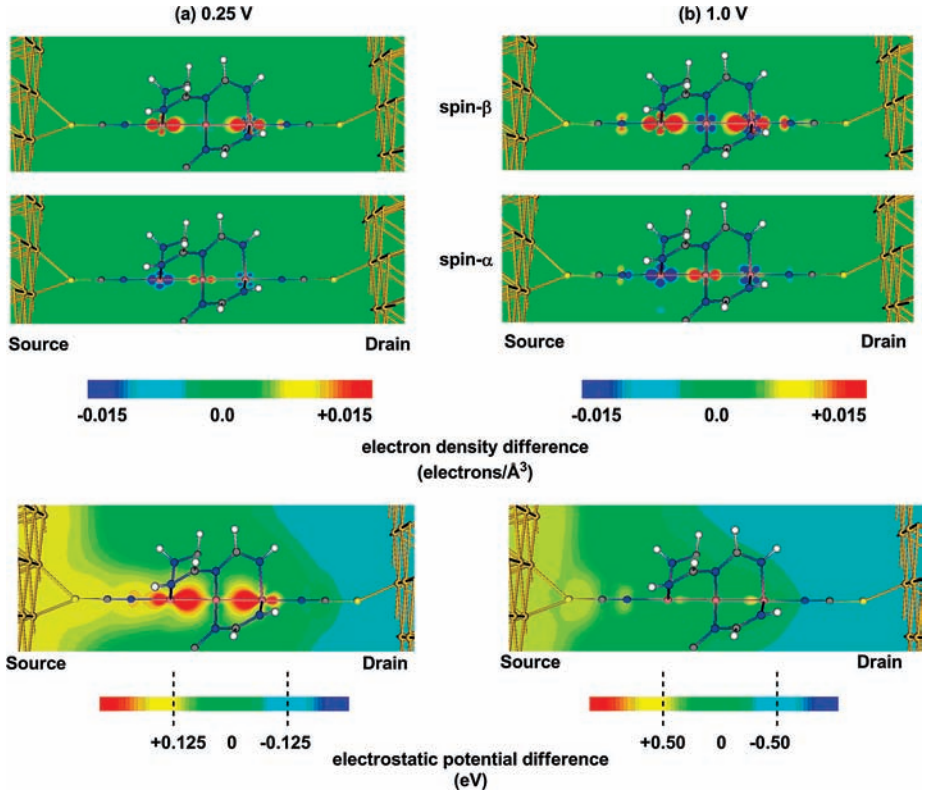

Figure 5. Charge redistribution (ρ(finite bias) − ρ(0 V)) and electrostatic potential profiles (V(finite bias) − V(0 V)) for [Au_{32}]-$Co_3(L)_4(NCS)_2$-[Au_{48}] at (a) 0.25 V and (b) 1.0 V.

Conclusions

In summary, our calculations suggest that the dominant electron transport channel in $Co_3(L)_4(NCS)_2$ is the σ nonbonding orbital, which is singly occupied in the doublet ground state of the isolated molecule. The excess of spin-α density characteristic of the doublet ground state of the molecule is maintained in the two probe system, even under substantial applied biases, and the resultant exchange splitting places the vacant spin-β component of σ^{nb} much closer to the Fermi level than its occupied spin-α counterpart. The result is spin filtering efficiences of ∼95% at moderate bias. At higher voltages, the bias window captures the upper tail of the broadened π^* channel, leading to a depletion of charge, and the orbital energies follow the potential of the drain. The electric field also causes a substantial rehybridization of the π manifold; as a result, the individual orbitals become localized in the vicinity of the source or drain, effectively closing the channel. The σ^{nb} channel, in contrast, is far less polarizable due to a much greater splitting within the $\sigma/\sigma^{nb}/\sigma^*$ manifold and so remains unpertubed and able to support current flow even at moderately high bias. The presence of orthogonal σ and π channels in $Co_3(dpa)_4(NCS)_2$ offers a striking contrast to conventional organic materials, where only orbitals of π symmetry lie near the Fermi level. In the present case, the contact with the electrode is established through the π system, while current flow is dominated by the orthogonal σ system. The implication of this is that, even when the highly polarizable π channels are strongly rehybridized by the applied electric field, current flow is not affected.

Acknowledgment. We acknowledge financial support from the EPSRC (EP/F019327/1).

Supporting Information Available: (1) A full set of Cartesian coordinated for the scattering region and (2) a comparison of the molecular orbital arrays of $Co_3(dpa)_4(NCS)_2$ and the truncated system, $Co_3(L)_4(NCS)_2$. This material is available free of charge via the Internet at http://pubs.acs.org.